

Investigating tropospheric effects and seasonal position variations in GPS and DORIS time-series from the Nepal Himalaya

Mireille Flouzat,¹ Pierre Bettinelli,¹ Pascal Willis,^{2,3} Jean-Philippe Avouac,⁴ Thierry Hérítier¹ and Umesh Gautam⁵

¹CEA, DAM, DIF, F-91297 Arpajon, France. E-mail: mireille.flouzat@cea.fr

²Institut Géographique National, Direction Technique, Saint-Mandé, France

³Institut de Physique du Globe de Paris, Géophysique Spatiale et Planétaire, Paris, France

⁴Tectonics Observatory, California Institute of Technology, Pasadena, CA 91125, USA

⁵Department of Mines and Geology, National Seismological Center, Lainchaur, Kathmandu, Nepal

Accepted 2009 May 13. Received 2009 April 16; in original form 2009 February 9

SUMMARY

Geodetic time-series from continuous GPS (cGPS) and 1 DORIS stations across the Himalaya of central Nepal show strong seasonal fluctuations observed on the horizontal and vertical components. Because the fluctuations determined at the different stations have similar phase but different amplitudes, these observations would imply that the secular shortening across the range is modulated by a seasonal strain. Given the geographic and climatic setting, there is however a possibility that the GPS positions be biased by tropospheric effects. We process these data using two different software packages and two different analysis strategies. Our analysis shows evidence for 1-strong seasonal fluctuation of zenithal delays consistent with *in situ* meteorological data and two strong horizontal tropospheric gradients in particular in the EW direction, that is, parallel to the mountain front at Gumba, also detected in DORIS results. We show that the tropospheric effects cannot however be the source of the observed seasonality of horizontal strain. This study supports the view that the seasonal strain in the Himalaya is real and probably driven by seasonal surface load variations. Our study adds support to the view that seasonal variations of seismicity in the Himalaya reflects seasonal variations of geodetic strain.

Key words: Time series analysis; Satellite geodesy; Transient deformation; Ionosphere/atmosphere interactions; Hydrology; Asia.

1 INTRODUCTION

Geodetic time-series often exhibit temporal variations (Blewitt *et al.* 2001). These variations may reflect the viscoelastic response of the lithosphere to surface loading related to continental water storage (Bawden *et al.* 2001; van Dam *et al.* 2001), atmospheric pressure (Kaniuth & Vetter 2005), snow accumulation (Heki 2001) or to transient deformation events, including earthquakes and slow slip events (e.g. Dragert *et al.* 2001; Douglas *et al.* 2005). Prominent temporal variations are in particular observed in horizontal and vertical geodetic time-series from the Nepal Himalaya and could reflect such processes (Bettinelli *et al.* 2006, 2008, Fig. 1). The time-series include strong seasonal fluctuations in addition to the secular rate related to the 19 ± 2.5 mm yr⁻¹ shortening across the Himalaya (Bettinelli *et al.* 2006; Bettinelli 2007). These variations are observed on all three-components (Figs 2 and 3) and may reflect seasonal strain potentially driving the seasonal variation of seismicity that was recently reported (Bollinger *et al.* 2007; Bettinelli *et al.* 2008).

Whether variations observed in GPS time-series positions reveal real ground deformation or processing artefacts is therefore an important issue to address a number of solid earth problems. This problem is largely explored through a peering approach at a global scale, (Dong *et al.* 2002). Locally, bias in periodic horizontal signals has been recognized to be related to unmodelled vertical signals (King *et al.* 2003). Atmospheric effects are among one of the dominant source of errors on GPS geodetic positions, and may severely limit the possibility to detect temporal variations. If not correctly modelled, atmospheric effects can indeed bias vertical positions (e.g. Beutler *et al.* 2001), but also horizontal positions in presence of atmospheric anisotropy, in particular humidity (Bar-Sever *et al.* 1998). The accuracy to which tropospheric effects are estimated and corrected has improved over the years but the possibility for bias probably remains (Davis *et al.* 1985; Beutler *et al.* 1989; Sjöberg 1992; Bock & Doerflinger 2001). It is now recognized that GPS data can be a reliable source of information on the tropospheric water content, as demonstrated from a number of methodological studies over the last 10 yr (e.g. Walpersdorf *et al.* 2007). As a matter

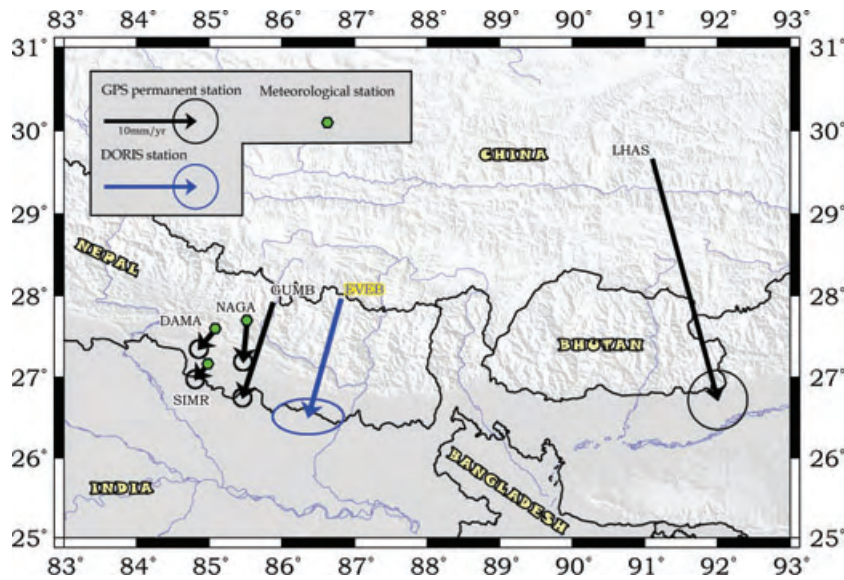


Figure 1. Location of the cGPS stations and meteorological stations analysed in this study. Black vectors show secular velocities relative to stable India determined by Bettinelli *et al.* (2006). The secular velocity at the DORIS station near Mount Everest (blue vector) and the LHAS station are also shown for comparison.

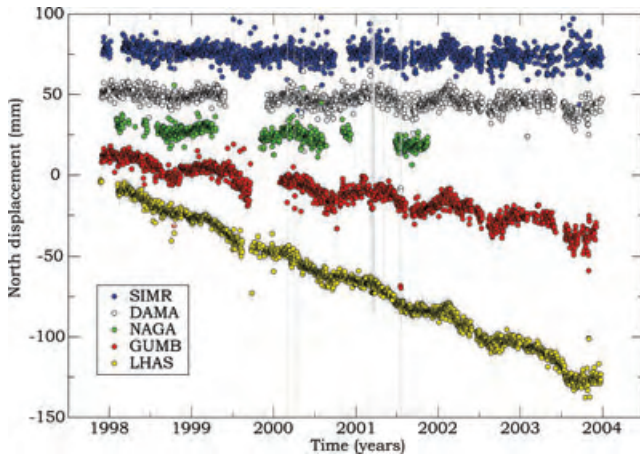


Figure 2. North component time-series of the five cGPS stations discussed in this study. Positions were determined relative to the Indian plate as defined by (Bettinelli *et al.* 2006). Error bars correspond to 1σ uncertainties. See Fig. 1 for location of stations.

of fact, dense networks of continuous GPS (cGPS) stations make it possible to carry on tropospheric tomography studies (Flores *et al.* 2000; Walpersdorf *et al.* 2004; Nilsson *et al.* 2007), or to correct efficiently atmospheric artefacts in interferometric synthetic radar images (Li *et al.* 2005).

In this study, we focus on tropospheric effects and the potential biases that they may induce on geodetic positions in the Himalayan region where the Monsoon regime induces particularly large fluctuations of tropospheric water content. We use data from four continuous GPS stations, which have been in operation across the Himalaya of central Nepal since 1997 (Bettinelli *et al.* 2006), and from the IGS station (Dow *et al.* 2005) near Lhasa (Fig. 1). We also use data from the DORIS station deployed at Mount Everest base camp as a permanent tracking station of the International DORIS Service (IDS, Tavernier *et al.* 2006). Given the increase in topography across the range, the quite abrupt contrast between the humid foreland to the arid Tibet plateau and the monsoon regime (Barros & Lang 2003;

Jade *et al.* 2005; Bookhagen & Burbank 2006), the potential for seasonal tropospheric artefacts is high.

Hereafter, we first describe the dataset assembled for this study and the processing strategy adopted to highlight the influence of tropospheric effects and possible potential processing bias. Next, we describe the results, compare the tropospheric delays estimated from the GPS data with the tropospheric water content estimated from *in situ* meteorological data, and discuss the eventual impact of tropospheric effects on geodetic positions. The study shows that the seasonal geodetic signal reported by Bettinelli *et al.* (2008) cannot be explained by mismodelling of tropospheric delays and reflect real geodetic strain and that this geodetic deformation is induced by surface load variations associated with the hydrological cycle.

2 DATA

Three permanent GPS stations, SIMRA, DAMAN and GUMBA (Fig. 1) were installed in 1997 by the DASE/LDG and the Department of Mines and Geology (DMG) of Nepal and have been operating nearly continuously since then. These data are freely available on the Tectonics Observatory website (<http://www.tectonics.caltech.edu/>). All measurements were made with Ashtech-sensor dual-frequency geodetic receivers and using choke-ring antennas to mitigate possible multipaths effects. The sampling rate was 30 s. Stations Daman and Gumba are installed directly on bedrock. Station Simra, in the Teraï, is settled on alluvium but it is this latter station which undergoes the smallest horizontal seasonal variations, as will be shown later. This dataset was previously analysed by Bettinelli *et al.* (2006) with data from: (1) the cGPS station NAGA deployed near Nagarkot by CIRES (University of Colorado) and the Survey of Nepal, which has been in operation sporadically between 1997 and 2001, (2) the DORIS station (Tavernier *et al.* 2006) near Mount Everest and (3) all available GPS campaigns (Jouanne *et al.* 1999, 2004; Larson *et al.* 1999).

We also used data from a DORIS station (EVEB) close to Mount Everest base camp in Nepal (Fig. 1). These data are freely available on the IDS Web site at <http://ids.cls.fr/html/doris/>

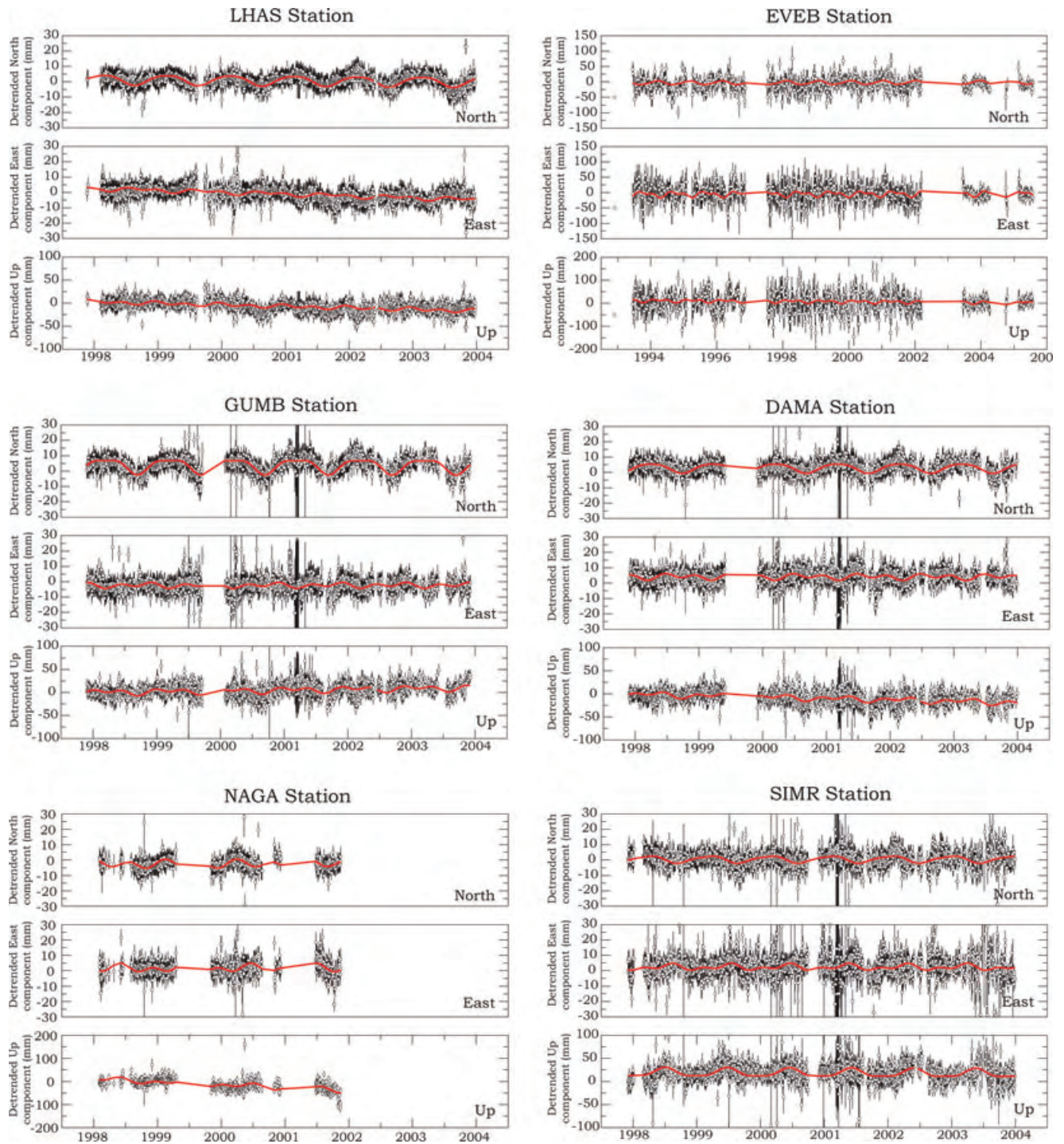


Figure 3. Observed NS, EW and vertical daily positions at stations SIMR, DAMA, GUMB, NAGA and LHAS (EVEB is expressed in weekly positions). The time-series were detrended by removing the secular motion of each station as determined by Bettinelli *et al.* 2006, from least-squares adjustment of the time-series with eq. (2). Note the change in the maximum units of the scale for the vertical component.

ids-station-series.php3. This station is using a Starec antenna and is installed on bedrock. It is in continuous operation since 1992 May 22 as part of the permanent DORIS tracking network (Fagard 2006).

We determine velocities in ITRF2000 (Altamimi *et al.* 2002) and next relative to the stable Indian plate (Figs 2 and 3), as defined by Bettinelli *et al.* (2006), using data from 19 additional regional IGS stations (Table 1).

3 DATA PROCESSING

To investigate the sensitivity of the results to the choice of the software package and to the processing approaches, we processed the GPS data with two different software packages (Bernese software from University of Bern and GIPSY/OASIS from Jet Propulsion Laboratory), using different tropospheric strategies.

Table 1. List and locations of GPS and DORIS stations of the Nepal network processed in this study, and IGS stations taken into account in the processing. Also reported is the DOMES number (International Terrestrial Reference Frame) of the IGS stations.

Station	Network	Longitude (°)	Latitude (°)	Altitude (m)
DAMA	GPS-CEA	85.107	27.608	2151
EVEB	DORIS	86.813	27.953	5050
GUMB	GPS-CEA	85.887	27.909	2899
NAGA	GPS-CIRES	85.521	27.693	2105
SIMR	GPS-CEA	84.984	27.165	71
IGS acronym	DOMES number	Longitude (°)	Latitude (°)	Altitude (m)
BAHR	24901M002	50.608	26.209	−17
BAKO	23101M002	106.849	−6.491	158
BJFS	21601M001	115.892	39.609	87
DGAR	30802M001	72.370	−7.270	−65
IISC	22306M002	77.570	13.021	844
IRKT	12313M001	104.316	52.219	503
KIT3	12334M001	66.885	39.135	643
KSTU	12349M002	92.794	55.993	210
KUNM	21609M001	102.797	25.030	1986
LHAS	21613M001	91.104	29.657	3622
MALD	22901S001	73.526	4.189	−92
NTUS	22601M001	103.680	1.346	79
POL2	12348M001	74.694	42.680	1714
SEY1	39801M001	55.480	−4.674	538
SHA0	21605M002	121.200	31.100	22
TAIW	23601M001	121.537	25.021	45
URUM	21612M001	87.601	43.808	856
WUHN	21602M001	114.357	30.531	25
XIAN	21614M001	109.221	34.369	82

3.1 Bernese data processing using network approach

All available cGPS measurements were initially processed (Bettinelli *et al.* 2006), using the Bernese V4.2 software (Beutler *et al.* 2001). Results were obtained directly in the ITRF2000 reference frame (Altamimi *et al.* 2002), using IGS final precise orbits (Beutler *et al.* 1999), and Earth Orientation Parameters (EOPs). We used a cut-off elevation angle of 10°. The antenna phase centre offsets and the phase centre corrections were computed using the models provided by the IGS (National Geodetic Survey web site <http://www.ngs.noaa.gov/>). We determined a free network solution. The carrier-phase ambiguities were determined using the following steps: an initial ionosphere-free analysis; resolution of the wide-lane ambiguities using the Melbourne–Wübbena linear combination depending on the quality of the code measurements (Melbourne 1985; Wübbena 1985); and finally a computation of the ionosphere free solution introducing the resolved Melbourne–Wübbena linear combination ambiguities. To account for the troposphere delay corrections (written as the product of the delay in zenith direction and a mapping function) we used the same standard cosZ mapping functions for the dry and the wet part delays. The wet part of the troposphere zenith delays were estimated from the observations every 2 hr and from the *a priori* Saastamoinen model (1974), using standard piecewise parametrization.

We computed daily station coordinate files in SINEX format (Blewitt *et al.* 1995), including a complete covariance information matrix. We then combined these independently processed daily so-

lutions using the quasi-observation combination analysis (QOCA) software (Dong *et al.* 1998; also see <http://gipsy.jpl.nasa.gov/qoca/>). The QOCA modelling of the time-series data was done through sequential Kalman filtering, transforming initial results into free-network solutions and allowing adjustment of global parameters, such as translations and rotations of the terrestrial reference frame, EOPs of each daily solution. Random-walk-style perturbations were allowed for some parameters whose errors were found to be correlated with time (e.g. EOPs and the antenna heights at a few sites). For more details about this procedure and estimation of uncertainties, the reader is referred to Shen *et al.* (2000) and <http://gipsy.jpl.nasa.gov/qoca/>. Time-series of stations coordinates were derived from this procedure to ensure a proper alignment of the daily realizations of the terrestrial reference system of the original Bernese results.

3.2 GIPSY/OASIS using PPP approach

We also processed all the GPS data using the GIPSY/OASIS in a very different mode, using this time a Precise Point Positioning (PPP) technique (Zumberge *et al.* 1997). We used the more recent GMF model for the tropospheric mapping function (Boehm *et al.* 2006) and estimated horizontal tropospheric gradients at each station. GPS data at a lower elevation than in the Bernese processing were also used (cut-off angle was 7°). The horizontal tropospheric gradient takes care of the possible asymmetry of the local atmosphere (few metres above the ground and up to 1–5 km maximum) at time scale of few minutes to a day and can be modelled as below, using the same conventions as Bar-Sever *et al.* (1998)

$$D_L = m_h(e) D_{hz} + m_w(e) D_{wz} + m_\Delta(e) \cot(e) [G_N \cos(\phi) + G_E \sin(\phi)], \quad (1)$$

where D_L is the tropospheric delay in the line of sight (satellite to ground station), e is the elevation of the satellite above the local horizon, as seen by the ground station, m_h is the hydrostatic mapping function (GMF in our example), D_{hz} is the total zenith hydrostatic delay, m_w is the wet mapping function), D_{wz} is the zenithal wet delay, $m_\Delta = m_w$ (GMF in our case), G_N and G_E is the tropospheric gradients (respectively in the south–north and west–east directions), and ϕ the azimuth.

In our GIPSY/OASIS GPS data processing, D_{wz} , G_N and G_E are estimated every 5 min as randomwalk variables, using tight constraints compatible with regular atmospheric conditions.

Furthermore, several studies have shown that the tropospheric gradient improves the ZTD estimation (Iwabuchi *et al.* 2003) and that influence of tropospheric effects on horizontal components can be mostly removed, and repeatability improved (Miyazaki *et al.* 2003). Anisotropy in the lower atmosphere cannot be completely modelled only by ZTDs. In such a case, remaining errors would naturally map into GPS residuals (Champollion *et al.* 2004). This approach is more rigorous and GPS-results were previously compared by previous authors to other sources of information such as VLBI or Water vapour radiometer (Gradinarsky *et al.* 2000; Snajdrova *et al.* 2006) showing good agreement. In our study, the estimated gradients are well determined and found significant when compared to their formal error. For one of the station (GUMBA), the horizontal gradients, when studied over the full period of data (1998.0–2005.0) show a significant offset from zero in the west direction (Fig. 5), parallel to the Himalaya chain. This offset is statistically significant and could reflect transport of moisture by E–W winds forced by the E–W striking front of the High Himalaya range which rises up

just north of the station). To our knowledge, no systematic study has been made to interpret such horizontal tropospheric gradients in terms of meteorology and systematic direction of moisture transport. Our explanation is only tentative and should be considered with caution since other causes might be advocated. For example multipath may also map into this estimated parameter. Finally, we also had a close look at our GPS residuals over the observed time span. They do not show any strong seasonal variations, which could be a sign of tropospheric mismodelling.

3.3 DORIS data processing

The DORIS data from EVEB station (91 km northeast of GUMB) were processed using the GIPSY/OASIS software by the IGN/JPL analysis group (Willis *et al.* 2006). This solution takes advantage of the latest analysis improvements described in Willis *et al.* (2007). Results for all DORIS stations are also freely available on the IDS website at <http://ids.cls.fr/html/doris/ids-station-series.php3>.

For consistency with the processing of the GPS data, we also estimated horizontal tropospheric gradients for using the data from 2007. This analysis also shows a significant non-zero estimation in the west direction, however with a smaller amplitude (1.5 mm at EVEB using the DORIS data versus 3.0 mm at GUMB using the GPS data). The DORIS tropospheric gradients are noisier (typically 1.5 mm for a daily estimation), but they are sufficiently precise to detect a clear offset from a zero value (that would correspond to a total anisotropy of the atmosphere), using almost a year of daily solutions. These results confirm that the GPS tropospheric gradients are probably related to a tropospheric anisotropy rather than to a local multipath problem.

4. RESULTS

4.1 Temporal variations of geodetic positions and strain

Besides a secular trend related to tectonics, the continuous GPS and DORIS time-series show obvious seasonal variations over the 7 yr

covered by the data (Figs 2 and 3). Although the GPS data strategies are very different in our Bernese and GIPSY/OASIS solutions, the resulting time-series show very similar linear trends and seasonal variations (Figs 6 and 7). The seasonal variations are particularly prominent on the northern component, that is, in the direction perpendicular to the Himalayan range. Calculated on the raw signals, the mean peak to peak amplitudes resulting from the Bernese and the GIPSY/OASIS data processing are of the same order, respectively, 21 and 24 mm on the north component of GUMBA, 17.2 and 16.1 mm for DAMA, 13.5 and 15.5 mm for LHASA. In order to enhance and characterize the seasonal variations, we removed the best-fitting secular rate (Fig. 3). To do so, we have adjusted the time-series with an analytical function (Yoshioka *et al.* 2004), which considers that the fluctuations are reasonably well adjusted from a sine function and its first harmonics

$$y(t) = a + b \times t + c \sin\left(\frac{2\pi t}{T} + \phi_1\right) + d \sin\left(\frac{4\pi t}{T} + \phi_2\right), \quad (2)$$

where b is the secular rate, c , T and ϕ_1 are the amplitude, period and phase of the periodic perturbations (\sim annual) and d and ϕ_2 the amplitude and phase of its second harmonics (\sim semi-annual). This formulation is appropriate given the obvious quasi-annual component, the small interannual variability and the quasi-harmonic shape of the annual perturbation. It yields a very good fit to the time-series (Fig. 3 and Table 2) with the period of the fluctuation being close to annual. The semi-annual terms are much smaller than the annual terms by almost an order of magnitude and very often not significant (Table 2). We observe that peak to peak amplitudes, resulting of this adjustment, of the annual term decreases from north to south, being of the order of 2.5 ± 1.7 mm at SIMR, 6 ± 0.6 mm at DAMA, 5.9 ± 0.7 mm at NAGA, 9.6 ± 0.2 mm at GUMBA, 12.7 ± 1.6 mm at EVEB and 6.37 ± 0.2 mm at LHASA. These oscillations are more or less equivalent every year. The annual variations show in fact a saw tooth pattern, which cannot be matched exactly by a sine function. The durations of southward displacements also seem systematically longer than the duration of northward displacements. The semi-annual term helps to reproduce this feature but a

Table 2. Coefficients of eq. (1) used to fit the Bernese-derived geodetic time-series with account for seasonal variations.

Station	Component	b (mm.yr ⁻¹)	c (mm)	d (mm)	T (d)	ϕ_1 (d)	ϕ_2 (d)
LHAS	North	12.8 ± 1.0	6.37 ± 0.20	0.22 ± 0.06	365 ± 0.007	347 ± 2	76 ± 3
	East	45.3 ± 1.0	2.65 ± 0.10	0.08 ± 0.65	364 ± 0.010	165 ± 3	75 ± 4
	Up	7.6 ± 3.0	8.59 ± 0.10	-0.42 ± 0.22	364 ± 0.001	295 ± 2	14 ± 5
EVEB	North	23.5 ± 0.6	12.7 ± 1.60	0.19 ± 1.02	355 ± 0.020	341 ± 6	70 ± 6
	East	36.5 ± 1.2	20.1 ± 0.30	-0.69 ± 0.96	346 ± 0.003	159 ± 8	69 ± 7
	Up	-6.1 ± 4.1	14.8 ± 0.50	-1.76 ± 1.02	365 ± 0.004	320 ± 2	49 ± 8
GUMB	North	25.74 ± 0.3	9.60 ± 0.20	-0.63 ± 0.36	364 ± 0.004	358 ± 2	87 ± 5
	East	36.15 ± 0.3	3.97 ± 0.20	-0.32 ± 0.69	365 ± 0.008	178 ± 3	88 ± 6
	Up	4.4 ± 1.0	12.8 ± 0.04	-0.06 ± 0.10	365 ± 0.001	301 ± 5	30 ± 3
NAGA	North	30.13 ± 0.3	5.91 ± 0.70	-0.16 ± 0.40	410 ± 0.030	354 ± 3	83 ± 5
	East	35.08 ± 0.3	5.49 ± 1.20	-0.26 ± 4.40	374 ± 0.100	180 ± 2	90 ± 6
	Up	0.7 ± 1.0	13.1 ± 1.20	-0.65 ± 3.60	383 ± 0.008	202 ± 4	111 ± 5
DAMA	North	31.90 ± 0.3	6.01 ± 0.60	-0.28 ± 0.24	355 ± 0.007	343 ± 4	72 ± 4
	East	37.08 ± 0.3	4.57 ± 0.20	-1.04 ± 0.05	365 ± 0.007	163 ± 6	73 ± 5
	Up	0.6 ± 1.0	14.4 ± 0.20	-2.37 ± 0.30	355 ± 0.003	355 ± 4	84 ± 5
SIMR	North	32.75 ± 0.3	2.48 ± 1.7	0.21 ± 0.84	346 ± 0.200	335 ± 2	64 ± 4
	East	37.88 ± 0.3	4.60 ± 0.20	-0.65 ± 0.40	337 ± 0.007	155 ± 6	65 ± 4
	Up	0.30 ± 1.0	20.3 ± 0.80	4.54 ± 2.00	355 ± 0.007	101 ± 2	10 ± 2

Notes: Coefficients b correspond the velocity in mm yr⁻¹. Coefficients c and d correspond, respectively to the amplitudes of the annual and semi-annual periodic variations. Coefficient T , corresponds to the annual period, ϕ_1 the phase of the annual period and ϕ_2 the phase of the semi-annual period, expressed in days.

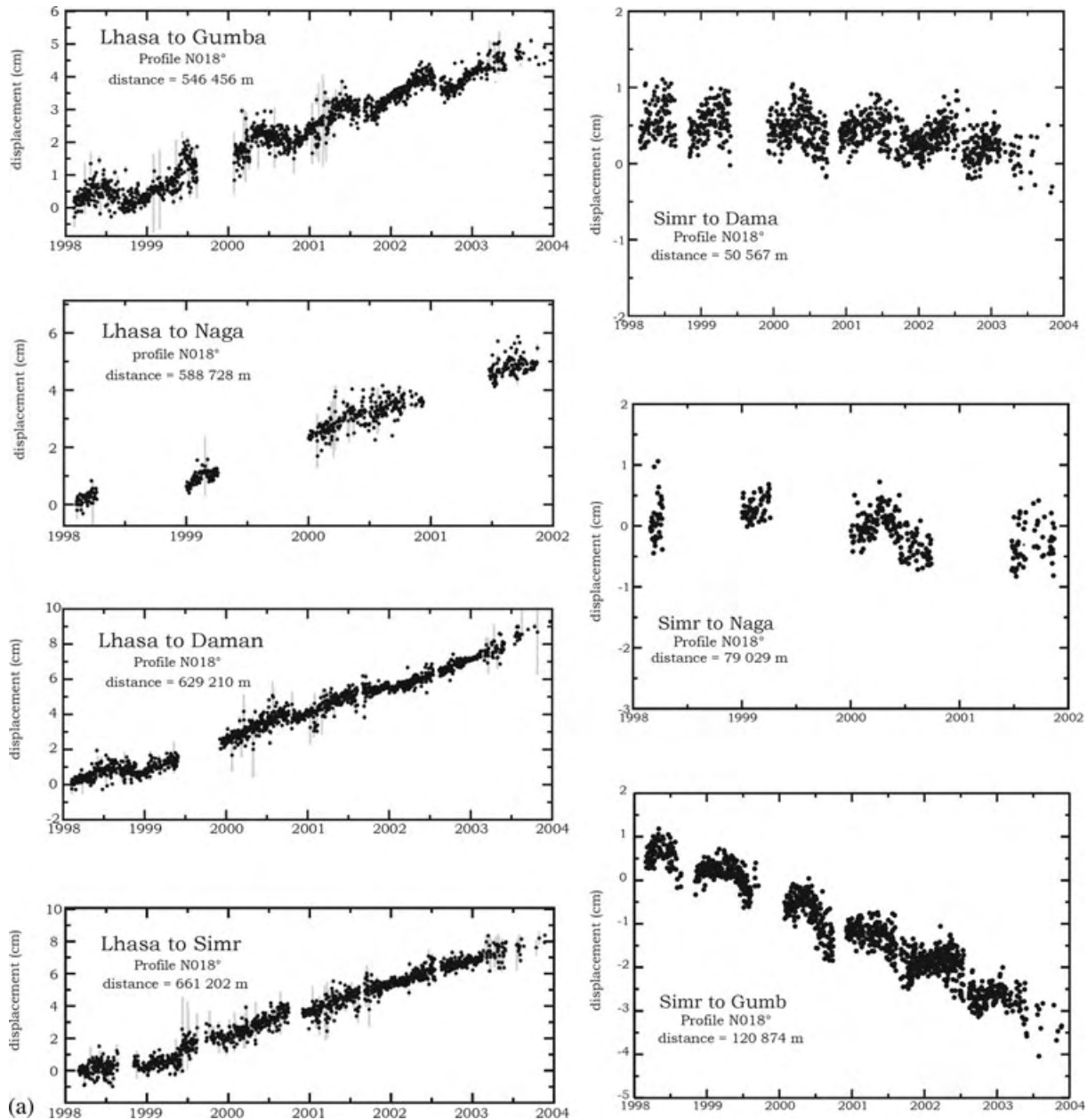


Figure 4. (a) Time-series showing the baselines length changes projected onto the N018° direction (approximate direction of convergence across the Himalaya of central Nepal) computed relative to LHASA (left-hand panel) and SIMR (right-hand panel). (b) Detrended time-series showing the baselines length changes projected onto the N018° direction (approximate direction of convergence across the Himalaya of central Nepal) computed relative to LHASA (left-hand panel) and SIMR (right-hand panel).

satisfying fit to the data can be obtained with only the annual term (Table 2).

4.2. Baseline approach

Several IGS stations have apparent seasonal variations, as detectable from SOPAC (e.g. SOPAC, see Williams *et al.* 2004, <http://sopac.ucsd.edu/processing/>: BAHN, WUHN). In principle, such a problem may affect station coordinates from a local network based on such IGS stations. To verify that our results do not depend on the fiducial network that we used, we also carried out a simpler baselines analysis of the regional network using only the four stations in Central Nepal and LHASA. These data were processed with Bernese. Strong seasonal variations show up on all baselines,

in particular for the baseline LHASA to GUMBA (Figs 4a and b). This is clear indication that a reference frame bias cannot explain the observed seasonality of our GPS time-series.

4.3. Comparison of GPS solutions with and without horizontal tropospheric gradients

The total zenith tropospheric delays estimated from the inversion of the GPS data using Bernese data processing are shown in Fig. 8. Tropospheric delay peaks in the summer are due to a dramatic increase in the percentage of moisture during the monsoon (Figs 8 and 9). It can be noted that the estimated ZTD consist of the followings.

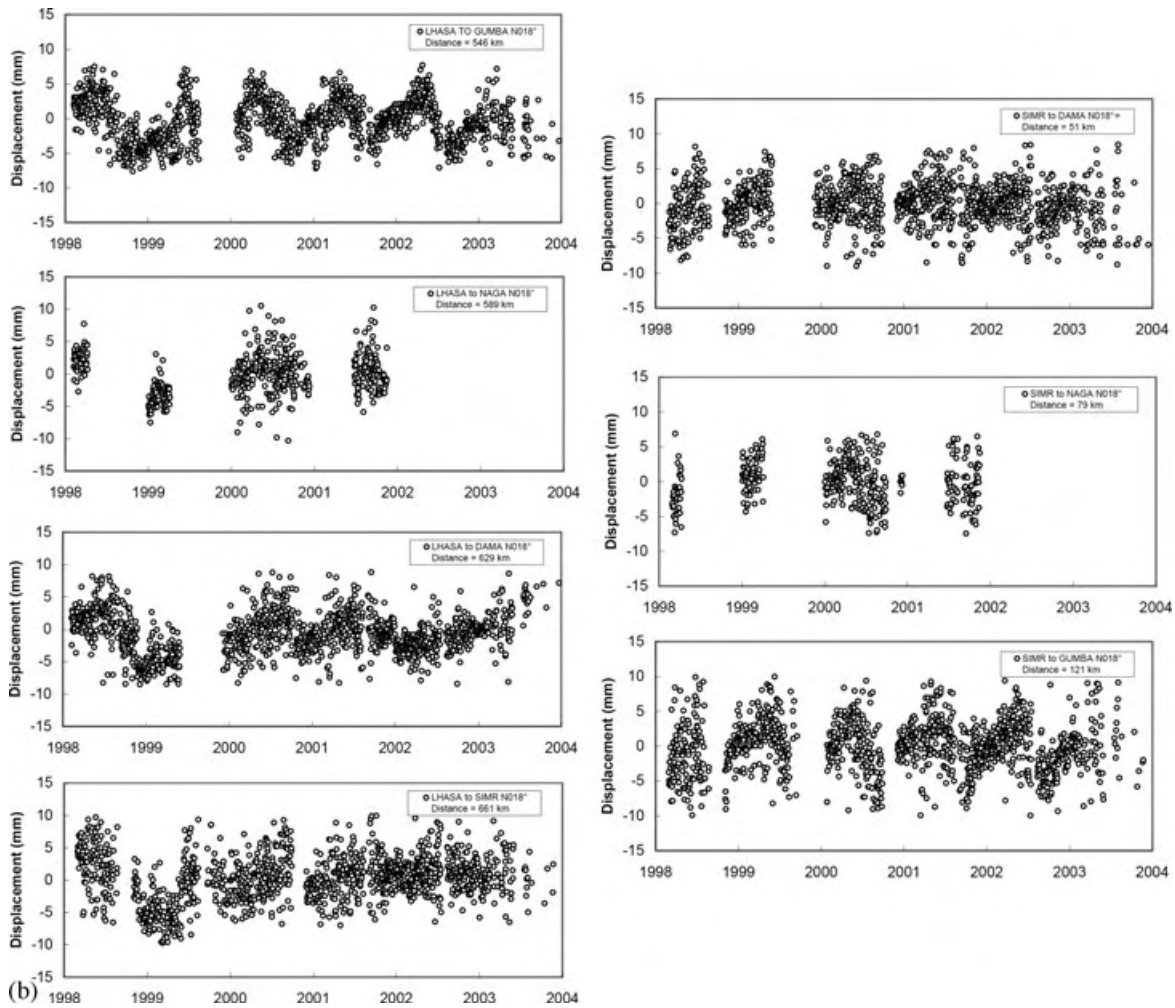


Figure 4. (Continued.)

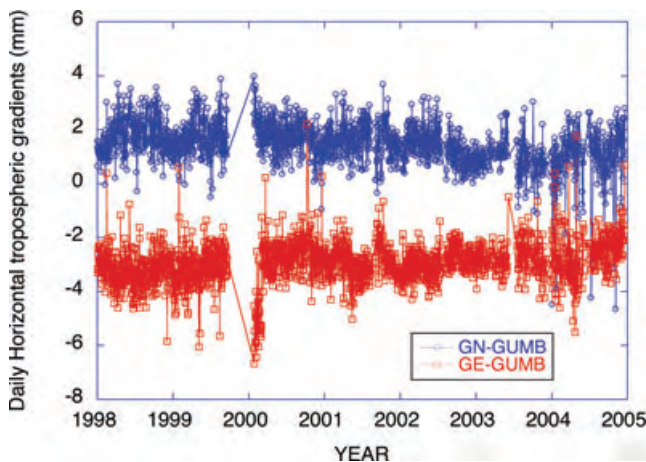


Figure 5. GPS horizontal tropospheric gradients derived at Gumba station (GUMB), using a PPP technique. 1 point corresponds to a 5-min data interval. All data were used (1998.0–2005.0). GN and GE correspond, respectively to the north and east coefficients in eq. (1).

(1) A constant term, which depends mostly on altitude (the higher constant term is observed at the lowest station SIMR, the smaller at the highest, LHASA). This constant term is probably driven by the dry component of the tropospheric delay, which can

be approximated, combining formulas from Davis *et al.* (1985), Elgered *et al.* (1991) and perfect gas laws, by

$$ZTD_{\text{dry}} = 1.013 \times 2.27e^{-0.000116h}, \quad (3)$$

where ZTD_{dry} is the dry tropospheric delay (in m), and h the altitude of the station (in m). This equation predicts an almost linear behaviour in the high altitude range of our stations due to the exponential decrease of the pressure with altitude.

(2) A seasonally varying term whose amplitude also depends on altitude (the larger amplitudes variations are obtained for the station at the lowest altitude, SIMR; and the smaller is obtained for the station with the highest altitude, LHASA) (see Table 3).

In order to evaluate the impact of analysis strategy on the ZTD determination, following Iwabuchi *et al.* (2003), we compare in Fig. 9 the ZTD determination from Bernese data processing (without any estimation of any horizontal tropospheric gradient) and GIPSY/OASIS (estimating a horizontal tropospheric gradient). We note that the amplitude of the seasonal variations are well above the differences between the two time-series (Table 4).

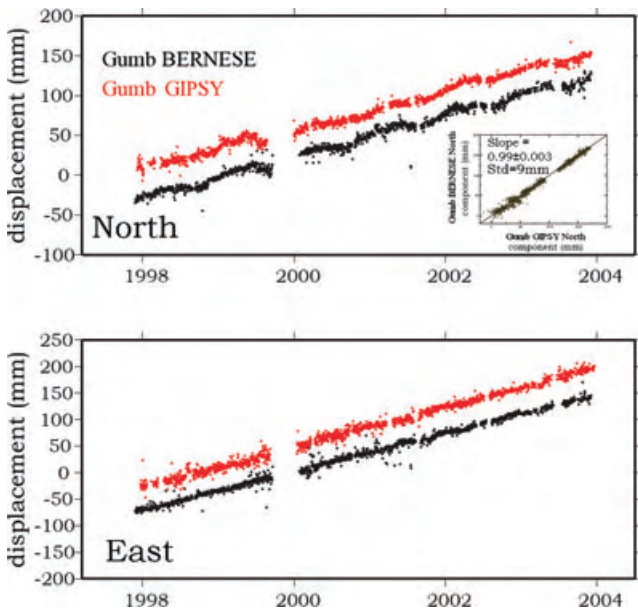


Figure 6. Position as a function of time determined relative to ITRF2000 at the GUMB cGPS station. Black dots show positions computed with BERNESE V4.2 in which only a vertical tropospheric gradient is inverted. Red dots show positions obtained from a Precise Point Positioning technique using GPS horizontal tropospheric gradients. Uncertainties are not shown here for clarity. The good agreement between the two time-series show that the seasonal variation is due neither to a processing artefact nor to an improper account for a horizontal tropospheric gradient (inset).

4.4. Comparison of zenith tropospheric delays with meteorological *in situ* measurements

Here we compare our ZTD estimates with estimates derived from *in situ* data (pressure, temperature and relative humidity) taking advantage of the availability of good quality local meteorological data. We were able to gather met data from stations close to SIMR (met station Bara, distance = 8 km), NAGA (met station Bhaktapur distance = 9 km) and DAMA (met station Makwanpur, distance = 27 km). Unfortunately, there is no meteorological station observing near our most northern GPS station (GUMB). From the available *in-situ* meteorological data, we computed equivalent tropospheric delays based on Saastamoinen (1974). As shown in Fig. 9, for all three stations NAGA, SIMR and DAMA, the GPS-derived ZTD agree quite well with the *in-situ* derived ZTD in terms of phase and amplitude, as well as for the constant term, while no *a priori* bias was removed in our comparison. The two estimates compare well with a mean difference on residuals of -0.05 , 0.001 and -0.006 m, and standard deviation of 0.07 , 0.03 and 0.05 m for stations SIMR, NAGA and DAMA, respectively. As expected, the mean difference and standard deviation values are higher for the station with the lower altitude, SIMR. The variations of the *in situ* meteorological data are consistent with variations from GPS-derived tropospheric delays.

The GPS-derived total zenith delay are indeed significantly correlated with the ZTD derived from the meteorological data (coefficient correlation and above 0.6 for DAMA and above 0.8 for NAGA and SIMR stations) (Table 5). This degree of correlation was unexpected as the surface meteorological data only represents the troposphere just above the station, while the GPS results integrate this information on the complete column from the station to the satellite. The lowest correlation is obtained for DAMA and cannot be interpreted as a dependency with station altitude as NAGA station is almost at

the same altitude. A closer look at the individual ZTD results of this station shows that the correlation is lower for this station due to a lowest correlation for extreme conditions (highest and lowest ZTD values, basically representing lowest and highest humidity conditions). The distance to the meteorological station is also the largest. In Table 5, only GPS Bernese ZTD estimations are considered as the correlation between Bernese and GIPSY derived ZTD is over 0.94.

The slope λ provided in Table 5 is computed as the average value over the full observation period, using the following simple formula:

$$ZTD_{Meteo}(t) = \lambda \cdot ZTD_{GPS}(t) + ZTD_0 \quad (4)$$

Table 5 shows that the estimated slope value are significantly different from 1 (except for the NAGA station), but not by an order of magnitude. This shows that even if the full tropospheric content of the column between the receiver on the ground and the satellite cannot be reliably predicted from the meteorological ground measurements, these two types of measurements do compare quite well in the Himalayan setting.

4.5 Comparison of temporal variations of zenith tropospheric delays and station positions

The comparison of the detrended station coordinate horizontal residuals with the total tropospheric delays shows that they are clearly not in phase (Fig. 10). Table 3 shows that the phase in the annual signal of the tropospheric delays is about 120 d and consistent for almost all stations in the GPS network. Table 2 shows that the annual signals observed in the station coordinates residuals are different from 120 d. Only SIMR vertical coordinates may be affected by an annual signal with a 120 d phase. However, station coordinates annual signals basically present a 350 d phase for north and 160 d for east, that is different in phase from the tropospheric annual signal. In addition, as demonstrated above, the tropospheric model has no significant influence on the amplitude of the seasonal horizontal variations. We conclude that the seasonal variations of station horizontal coordinates cannot be explained by mismodelling errors in the troposphere. Finally, the observed phase delay derived from the DORIS station coordinate time-series at Everest (EVEB) are very consistent with the GPS results (350 d for north and 160 d for east). In addition, the phase differences between the EW and NS are consistent with the model proposed by Bettinelli *et al.* (2008). The model does predict an elliptical seasonal trajectory at each station, and not a displacement along a line, because the spatial distribution of surface loading does vary with time leading to different phases on the EW and NS component.

5 CONCLUSIONS

Permanent geodetic monitoring in the Himalaya reveals that secular interseismic strain is modulated by strong seasonal variations observed in GPS and DORIS time-series. Although seasonal variations in GPS time-series are commonly observed and could arise form a variety of artefacts, the fact that it is better observed in the horizontal component than in the vertical component is a specific feature of this network. Baseline analysis shows that the observed seasonality is not an artefact of the densification procedure used to express position results in a well-defined terrestrial reference frame. Results obtained from processing the same GPS data using two different software packages (Bernese and GIPSY/OASIS), and adopting different analysis strategies for terrestrial reference realization and for tropospheric correction, show strong horizontal tropospheric gradients, probably reflecting orogenic forcing on

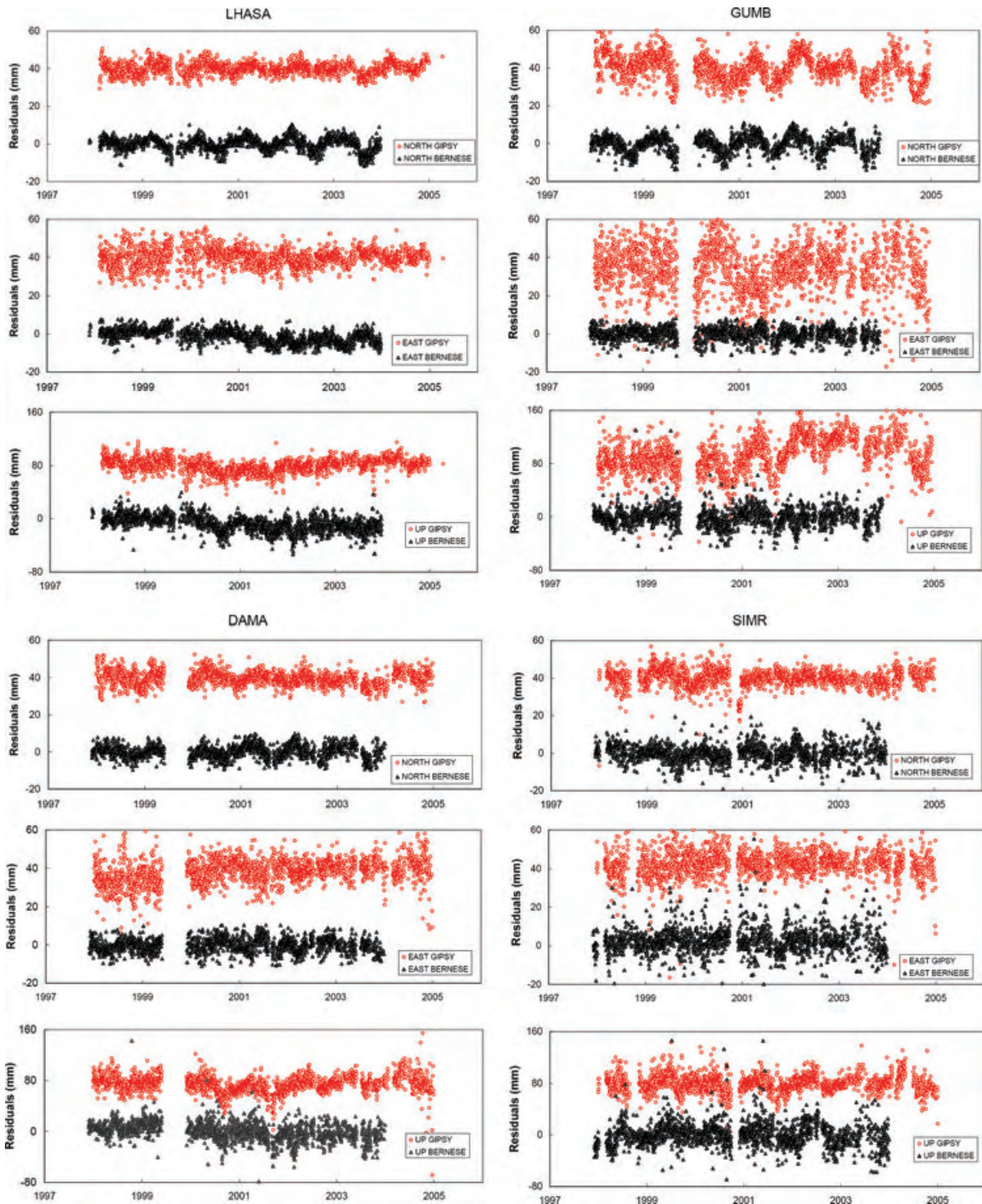


Figure 7. Position time-series obtained for cGPS stations from the two GPS data processing (Gipsy, red circles; Bernese, black triangles). The time-series are detrended using velocities from Bettinelli *et al.* (2006) for horizontal components. For clarity, the delays computed with GIPSY are offset by 40 mm for the horizontal components, and 80 mm for the vertical component. There is no ambiguity solution in the GIPSY PPP solutions, leading to a greater scatter, especially in the east component.

moisture transport, and seasonal variation of the total zenith delays in surprisingly good agreement with those predicted from *in situ* meteorological measurements.

Our analysis demonstrates that the observed horizontal annual signals are not an artefact of the GPS processing related with tro-

pospheric mismodelling. The amplitude of the horizontal seasonal geodetic displacements increases northwards, so that the shortening rate across the range is lower in the summer than in the winter. The geodetic data thus points to a local source capable of producing horizontal contraction in the winter and horizontal extension in the

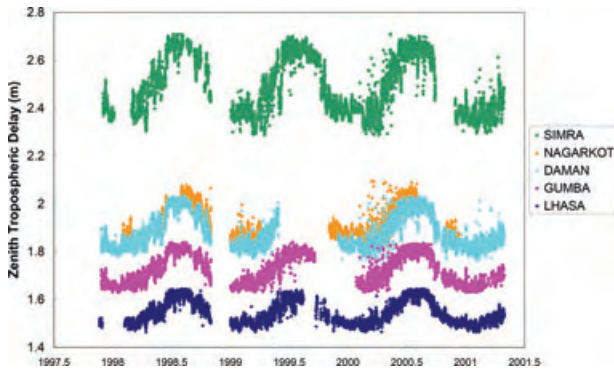


Figure 8. Time-series of total zenith tropospheric delays at the five cGPS stations analysed in this study obtained from the Bernese GPS data processing are presented here.

summer, superimposed on the secular shortening rate across the Himalaya. As proposed by Bettinelli *et al.* (2008) this pattern is consistent in phase and amplitude with the effect of surface load variation as estimated from GRACE and TOPEX/Poseidon data (Fig. 11). The observed and predicted variations show extension across the range (northward horizontal displacements relative to

stable India) to loading of the Ganges foreland basin by increasing water storage during the spring and summer and compression (southward horizontal displacements relative to stable India) in the Fall and Winter as the water storage decreases. The good agreement between the model and the GPS data both in amplitude and phase shows that the times series presented are not biased significantly by tropospheric artefact. This study shows that in certain favourable setting the effect of surface hydrology might be better detected on the horizontal components than on the vertical components. Our findings also add support to the view that the seasonal variations of seismicity observed in the Himalaya, the seismicity rate being twice higher in the Winter than in the Summer (Bollinger *et al.* 2007), are driven by seasonal variations of stressing rates, an observation that has important implications as to the mechanism of earthquakes nucleation (Bettinelli *et al.* 2008).

ACKNOWLEDGMENTS

We are most grateful to M.R. Pandey and all our collaborators, at NSC and DMG, and at CEA/DASE for their dedicated effort, which permitted the deployment, maintenance, and operation of the cGPS stations. This study has benefited from discussions with François

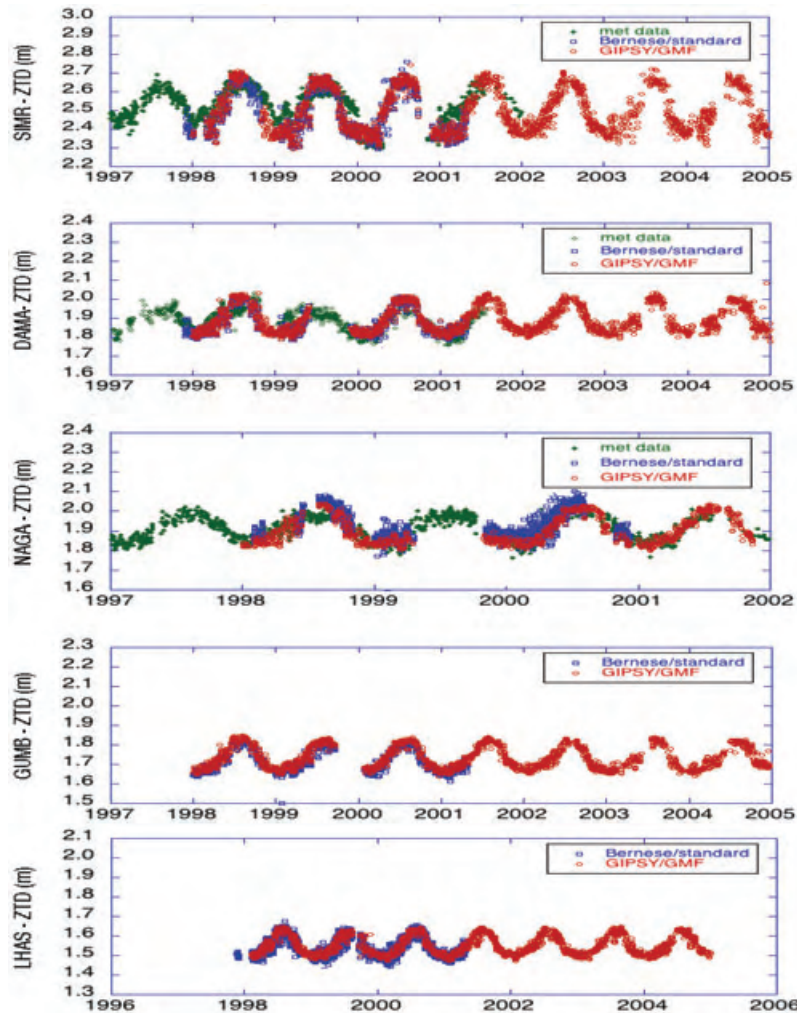


Figure 9. Comparison of time-series of total zenith tropospheric delays at the five CGPS stations analysed in this study obtained from the two GPS data processing Bernese (blue squares), and Gipsy/OASIS (red circles), and those calculated using meteorological data provided by the Nepal Department of Meteorology and Hydrology (green dots) and calculated from Saastamoinen 1974. See Fig. 1 for location of meteorological data.

Table 3. Coefficients of eq. (1) used to fit the zenith tropospheric delay time-series estimated from the Bernese data processing.

Station	c (m)	d (m)	T (d)	φ_1 (d)	φ_2 (d)	χ^2
Zenith Tropospheric Delay						
LHAS	0.112	0.004 ± 0.2	363	119 ± 2	29 ± 3	0.015
GUMB	0.150	0.010 ± 0.05	366	118 ± 5	39 ± 3	0.0009
NAGA	0.180	-0.008 ± 0.8	364	120 ± 4	32 ± 5	0.0018
DAMA	0.200	0.004 ± 0.2	362	120 ± 4	32 ± 3	0.002
SIMR	0.360	0.020 ± 1.5	360	125 ± 3	42 ± 5	0.038

Notes: Coefficients c and d correspond, respectively, to the amplitudes of the annual and semi-annual periodic variations. Coefficients T , φ_1 and φ_2 correspond, respectively, to the period and to the annual and semi-annual phases, expressed in days.

Table 4. Residuals between ZTD Gipsy and Bernese estimated solutions.

Station	Shift (m)	Standard deviation (m)
GUMB	0.0147	0.0075
DAMA	0.0040	0.0070
SIMR	0.0076	0.0092

Table 5. Comparison between Zenith Total Delay (ZTD) derived from surface meteorological data and GPS observation. Correlation coefficient and slope, λ , between the 2 ZTD time-series, as defined in eq. (4).

GPS station (acronym)	Altitude (m)	ZTD correlation (unitless)	Slope, λ (unitless)
DAMA	2,151	0.650	0.590 ± 0.046
NAGA	2,105	0.827	0.995 ± 0.033
SIMR	71	0.850	0.530 ± 0.038

Jouanne (LGCA, Université de Savoie, France), Christophe Vigny and Rodolphe Cattin (Ecole Normale Supérieure, ENS, Paris). We are grateful to Jeff Freymuller and Becky Bendick for constructive reviews of the manuscript. Roger Bilham A. Waldersporfs, K. Heki, and an anonymous reviewer also provided helpful comments on an earlier version of that manuscript. Part of this work was supported by the Centre National d'Etudes Spatiales (CNES). It is based on observations with DORIS embarked on SPOTs, TOPEX/Poseidon and ENVISAT satellites. This paper is IPGP contribution 2491 and Tectonic Observatory contribution 103.

REFERENCES

- Altamimi, Z., Sillard, P. & Boucher, C., 2002. ITRF2000: a new release of the International Terrestrial Reference Frame for Earth science applications, *J. geophys. Res.*, **107**(B10), 2214.
- Barros, A.P. & Lang, T.J., 2003. Monitoring the monsoon in the Himalayas: observations in Central Nepal, June 2001, *Mon. Wea. Rev.*, **131**(7), 1408–1427.
- Bar-Sever, Y.E., Kroger, P.M. & Borjesson, J.A., 1998. Estimating horizontal gradients of tropospheric path delay with a single GPS receiver, *J. geophys. Res.*, **103**(B3), 5019–5035.
- Bawden, G.W., Thatcher W., Stein R.S., Hudnut K.W. & Peltzer G., 2001. Tectonic contraction across Los Angeles after removal of groundwater pumping effects, *Nature*, **412**(6849), 812–815.
- Bettinelli, P., 2007. Déformation intersismique de l'Himalaya du Népal à partir de données GPS, *PhD thesis*. Université Paris VII, 198 pp.
- Bettinelli, P., Avouac, J.P., Flouzat, M., Jouanne, F., Bollinger, L., Willis, P. & Chitrakar, G.R., 2006. Plate motion of India and interseismic strain in the Nepal Himalaya from GPS and DORIS measurements, *J. Geod.*, **80**(8–11), 567–589.
- Bettinelli, P., Avouac, J.P., Flouzat, M., Bollinger, L., Ramillien, G., Rajaure, S. & Sapkota, S., 2008. Seasonal variations of seismicity and geodetic strain in the Himalaya induced by surface hydrology, *Earth planet. Sci. Lett.*, **266**, 332–334.
- Beutler, G., Bausersima, I., Botton, S., Gurtner W., Rothacher M. & Schildknecht T., 1989. Accuracy and biases in the geodetic application of the Global Positioning System, *manuscripta geodaetica*, **14**, 28–35.
- Beutler, G., Rothacher, M., Schaer, S., Springer, T.A., Kouba, J. & Neilan, R.E., 1999. The international GPS service (IGS): an interdisciplinary service in support of earth sciences, **23**(4), 631–653.
- Beutler, G. et al., 2001. *Bernese GPS Software Version 4.2 Astronomical Institute*, University of Berne, Berne.
- Blewitt, G., Bock, Y. & Kouba, J., 1995. Constructing the IGS polyhedron by distributed processing, in *Processing of the IGS Workshop*, pp. 31–36, ed. Zumberge, J., IGS Central Bureau, Pasadena.
- Blewitt, G., Lavalee, D., Clarke, P. & Nurutdinov, K., 2001. A new global mode of Earth deformation: seasonal cycle detected, *Science*, **294**(5550), 2342–2345.
- Bock, O. & Doerflinger, E., 2001. Atmospheric modeling in GPS data analysis for high accuracy positioning, *Phys. Chem. Earth. (A)*, **26**(6–8), 373–383.
- Boehm, J., Niell, A., Tregoning, P. & Schuh, H., 2006. Global Mapping Function (GMF): a new empirical mapping function based on numerical weather model data, *Geophys. Res. Lett.*, **33**(7), L07304.
- Bollinger, L., Perrier, F., Avouac, J.P., Sapkota, S., Gautam, U. & Tiwari, D.R., 2007. Seasonal modulation of seismicity in the Himalaya of Nepal, *Geophys. Res. Lett.*, **34**(8), L08304, doi:10.1029/2006GL029192.
- Bookhagen, B. & Burbank, D. W., 2006. Topography, relief, and TRMM-derived rainfall variations along the Himalaya, *Geophys. Res. Lett.*, **33**, L08405, doi:10.1029/2006GL026037.
- Champollion, C., Masson, F., Van Baelen, J., Walpersdorf, A., Chéry, J. & Doerflinger, E., 2004. GPS monitoring of the tropospheric water vapor distribution and variation during the 9 September 2002 torrential precipitation episode in the Cévennes (southern France), *J. geophys. Res.*, **109**, D24102, doi:10.1029/2004JD004897.
- Davis, J.L. Herring, T.A., Shapiro, I.I., Rogers, A.E.E. & Elgered, G. 1985. Geodesy by radio interferometry: effects of atmospheric modelling errors on estimates of baseline length, *Radio Sci.*, **20**(6), 1593–1607.
- Dong, D., Herring, T.A. & King, R.W., 1998. Estimating regional deformation from a combination of space and terrestrial geodetic data, *J. Geod.*, **72**(4), 200–214.
- Dong, D., Fang, P., Bock, Y., Cheng, M. & Miyazaki, S., 2002. Anatomy of apparent seasonal variations from GPS-derived site position time series, *J. geophys. Res.*, **107**(B4), 2075, doi:10.1029/2001JB000573.
- Douglas, A., Beavan, J., Wallace, L. & Townend, J., 2005. Slow slip on the northern Hikurangi subduction interface, New Zealand, *Geophys. Res. Lett.*, **32**(16), L16305, doi:10.1029/2005GL023607.

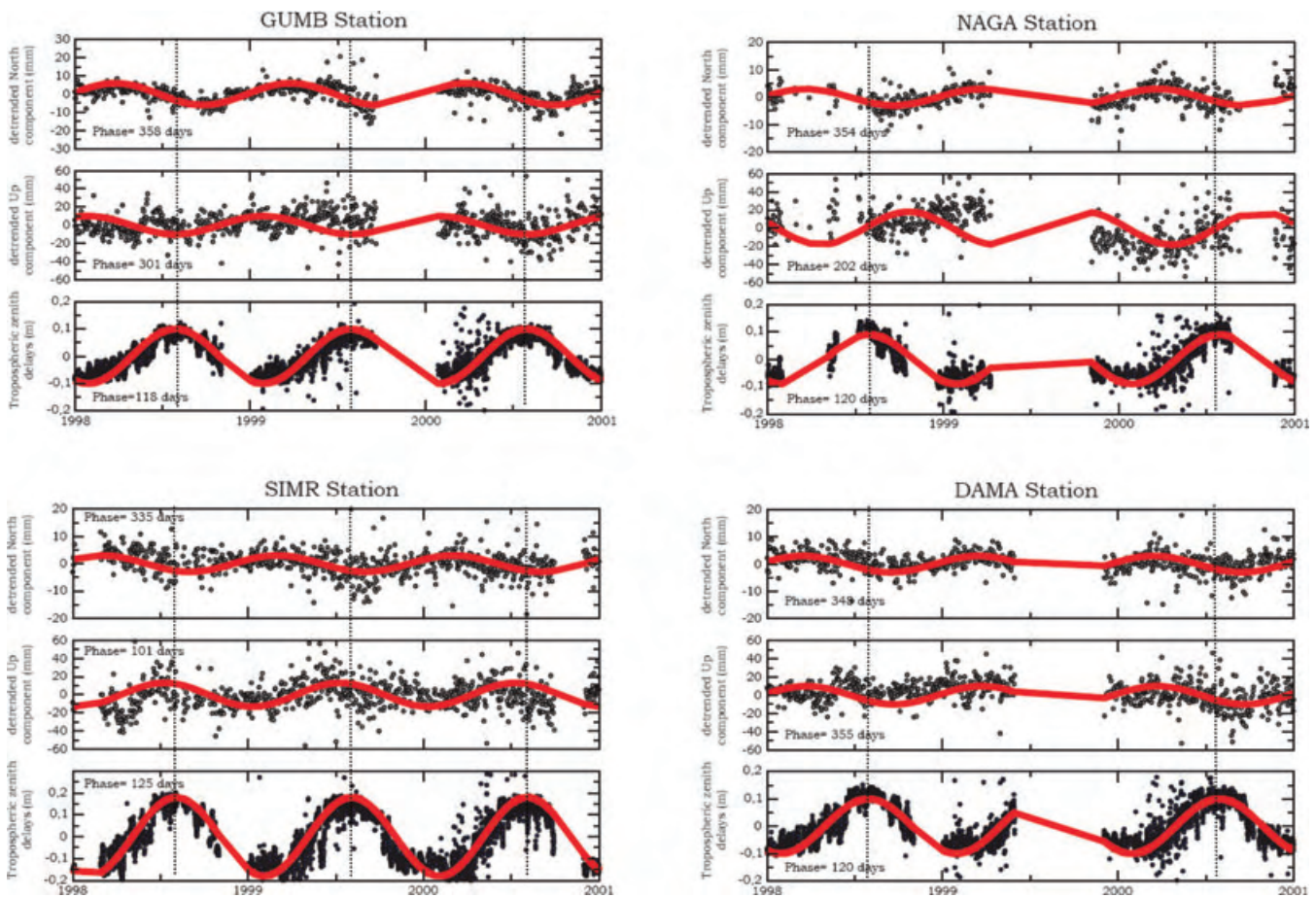


Figure 10. Detrended northward displacements, and vertical displacements at the four CGPS stations SIMR, DAMA, NAGA, GUMB (black dots). Total zenith tropospheric delays estimated during the processing with BERNESE V4.2 (bottom) are shown for comparison (black dots). Red lines correspond to the best fit with a sinus function (taking into account only the annual term). Vertical black lines show the pick of the tropospheric delay.

Dow, J.M., Neilan, R.E. & Gendt, G. 2005. The International GPS Service (GPS): celebrating the 10th anniversary and looking for the new decade, *Adv. Space Res.*, **36**(3), 320–326.

Dragert, H., Wang, K. & James, T.S., 2001. A silent slip event on the deeper Cascadia subduction interface, *Science*, **292**, 1525–1528.

Elgered, G., Davis, J.L., Herring, T.A. & Shapiro, I.I., 1991. Geodesy by Radio Interferometry: water vapor radiometry for estimation of the wet delay, *J. geophys. Res.*, **96**, 6541–6555.

Fagard, H., 2006. Twenty years of evolution for the DORIS permanent network: from its initial deployment to its renovation: in DORIS Special Issue, *J. Geod.*, **80**(8–11), 429–456.

Flores, A., Ruffini, G. & Rius, A., 2000. 4D tropospheric tomography using GPS slant wet delays, *Ann. Geophys.*, **18**(2), 223–234.

Gradinarsky, L.P., Haas, R., Elgered, G. & Johansson, J.M., 2000. Wet path delay and delay gradients inferred from microwave radiometer, GPS and VLBI observations, *Earth Planets Space*, **52**(10), 695–698.

Heki, K., 2001. Seasonal modulation of interseismic strain buildup in north-eastern Japan driven by snow loads, *Science*, **293**(5527), 89–92.

Iwabuchi, T., Miyazaki, S., Heki, K., Naito I. & Hatanaka, Y., 2003. An impact of estimating tropospheric delay gradients on tropospheric delay estimations in the summer using the Japanese nationwide GPS array, *J. geophys. Res.*, **108**(D10), 4315, doi:10.1029/2002JD002214.

Jade, S., Vijayan, M.S.M., Gaur, V.K., Prabhu, Tushar, P. & Sahu, S.C., 2005. Estimates of precipitable vapour from GPS data over the Indian subcontinent, *J. Atmos. Solar-Terres. Phys.*, **67**, 623–635.

Jouanne, F., Mugnier, J.L., Pandey, M.R., Gamond, J.F., Le Fort, P., Serrurier, L., Vigny, C. & Avouac, J.P., 1999. Oblique convergence

in the Himalayas of western Nepal deduced from preliminary results of GPS measurements, *Geophys. Res. Lett.*, **26**(24), 1933–1936.

Jouanne, F., Mugnier, J.L., Gamond, J.F., Le Fort, P., Pandey, M.R., Bollinger, L., Flouzat, M. & Avouac, J.P., 2004. Current shortening across the Himalayas of Nepal, *Geophys. J. Int.*, **157**(1), 1–14, doi:10.1111/j.1365-246X.2004.02180x

Kaniuth, K. & Vetter, S., 2005. Estimating atmospheric pressure loading regression coefficients from GPS observations, *GPS Solut.*, **9**(1), 32–40, doi:10.1007/s10291-005-0014-4.

King, M., Colemar, R. & Nguyen L.N., 2003. Spurious periodic horizontal signals in sub-daily GPS position estimates, *J. Geod.*, **77**(1–2), 15–21, doi:10.1007/s00190-002-0308-z.

Larson, K.M., Burgmann, R., Bilham, R. & Freymueller, J.T., 1999. Kinematics of the India-Eurasia collision zone from GPS measurements, *J. geophys. Res.*, **104**(B1), 1077–1093.

Li, Z.H., Muller, J.P., Cross, P. & Fielding E., 2005. Interferometric synthetic aperture radar (Insar) atmospheric correction: GPS, Moderate Resolution Imaging Spectroradiometer (MODIS), and InSAR integration, *J. geophys. Res.*, **110**(B3), B03410, doi:10.1029/2004JB003446.

Melbourne, W.G., 1985. The case for ranging in GPS based geodetic system, in *Proceedings of the 1st International Symposium on Precise Positioning with Global Positioning System*, pp. 373–386, ed. Goad, C. US Department of Commerce, Rockville, MD.

Miyazaki, S., Iwabuchi, T., Heki, K. & Naito, I., 2003. An impact of estimating tropospheric gradient on precise positioning in summer using the Japanese nationwide GPS array, *J. geophys. Res.*, **108**(B7), 2335, doi:10.1029/2000JB000113.

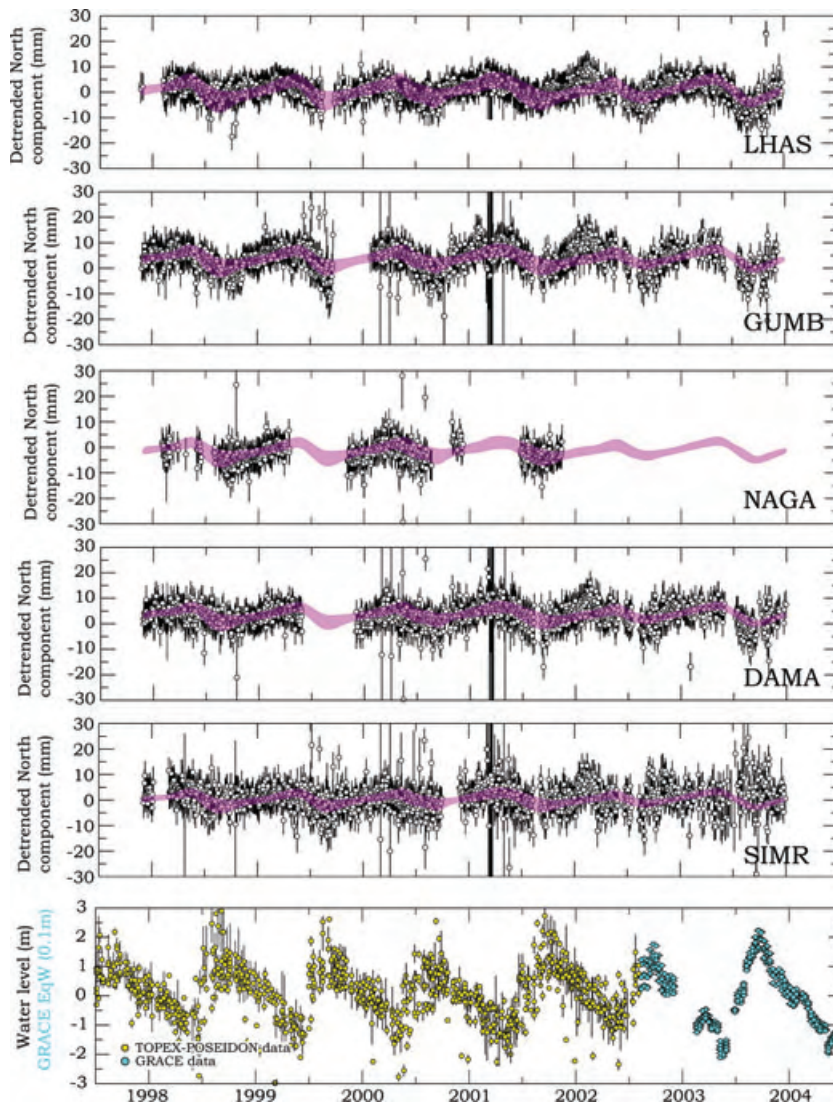


Figure 11. Comparison of seasonal variation of geodetic displacements and water level in the Ganges basin (bottom graph). Water level variations of some major rivers in the Ganges basin measured by Topex-Poseidon (yellow dots) and equivalent water thickness derived from GRACE (blue dots). Purple shaded areas show seasonal geodetic displacements computed from the variation of surface load due to seasonal variation of water storage (2σ uncertainty) assuming an elastic half-space with an elastic shear modulus of 40 GPa, and a Poisson coefficient of 0.25 (Bettinelli *et al.* 2008).

- Nilsson, T., Gradinarsky, L. & Elgered, G., 2007. Water vapour tomography using GPS phase observations: results from the ESCOMPTE experiment, *Tellus*, **59**(5), 674–682.
- Saastamoinen, J., 1974. Contributions of the theory of atmospheric refraction (part II), *Bull. Géod.*, **107**, 13–34.
- Shen, Z.K., Zhao, C.K., Yin, A., Li, Y.X., Jackson, D.D., Fang, P. & Dong, D.N., 2000. Contemporary crustal deformation in east Asia constrained by Global Positioning System measurements, *J. geophys. Res.*, **105**(B3), 5721–5734.
- Sjöberg, L., 1992. Systematic tropospheric errors in geodetic positioning with the global positioning system, *Manuscripta Geodetica*, **17**, 201–209.
- Snajdrova, K., Boehm, J. Willis, P. & Schuh, H., 2006. Multi-technique comparison of tropospheric zenith delays derived during the CONT02 campaign, *J. Geod.*, **79**(10–11), 613–623.
- Tavernier, G. *et al.*, 2006. The International DORIS Service, genesis and early achievements, *J. Geod.*, **80**(8–11), 403–417.
- van Dam, T., Wahr, J., Milly, P.C.D., Shmakin, A.B., Blewitt, G., Lavallee, D. & Larson, K.M., 2001. Crustal displacements due to continental water loading, *Geophys. Res. Lett.*, **28**(4), 651–654.
- Walpersdorf, A., Bock, O., Doerflinger, E., Masson, F., van Baelen, J., Somieski, A. & Bürki, B., 2004. Data analysis of a dense GPS network operated during the ESCOMPTE campaign: first results, *Phys. Chem. Earth*, **29**(2–3), 201–211.
- Walpersdorf, A., Bouin M.-N., Bock O. & Doerflinger E., 2007. Assessment of GPS data for meteorological applications over Africa: study of error sources and analysis of positioning accuracy, *J. Atmos. Solar-Terrest. Phys.*, **69**, 1312–1330.
- Williams, S.D.P., Bock, Y., Fang, P., Jamason, P., Nikolaidis, R.M., Prawirodirdjo, L., Miller, M. & Johnson, D.J., 2004. Error analysis of continuous GPS position time series, *J. geophys. Res.*, **109**, B03412, doi:10.1029/2003JB0022741.
- Willis, P., Jayles, C. & Bar-Sever, Y., 2006. DORIS: from altimetric missions orbit determination to Geodesy, *CR Geosci.*, **338**(14–15), 968–979.
- Willis, P., Soudarin, L., Jayles, C. & Rolland, L., 2007. DORIS applications for solid Earth and atmospheric sciences, *CR Geosci.*, **339**(16), 949–959.
- Wübbena, G., 1985. Software developments for geodetic positioning with GPS using TI 4100 code and carrier measurements, in *Proceedings of the*

1st International Symposium on Precise Positioning with the Global Positioning System, pp. 403–412, ed. Goad, C. US Department of Commerce, Rockville, MD.

Yoshioka, S., Mikumo, T., Kostoglodov, V., Larson, K.M., Lowry, A.R. & Singh, S.K., 2004. Interplate coupling and a recent aseismic slow slip event in the Guerrero seismic gap of the Mexican subduction zone, as

deduced from GPS data inversion using a Bayesian information criterion, *Phys. Earth planet. Inter.*, **146**(3–4), 513–530.

Zumberge, J.F., Heflin, M.B., Jefferson, D.C., Watkins, M.M., Webb, F.H., 1997. Precise point positioning for the efficient and robust analysis of GPS data from large networks, *J. geophys. Res.*, **102**(B3), 5005–5017.